A Simple Method To Valorize Silica Sludges Into Sustainable Coatings For Indoor Humidity Buffering

Chi-Hong Kuok
National Cheng Kung University
Wahid Dianbudiyanto
Universitas Airlangga
Shou-Heng Liu (shliu@mail.ncku.edu.tw)
National Cheng Kung University Department of Environmental Engineering https://orcid.org/0000-0002-4852-874X

Research

Keywords: Valorization, mesoporous/microporous structure, indoor humidity control, industrial sludges, sol-gel

Posted Date: September 15th, 2021

DOI: https://doi.org/10.21203/rs.3.rs-871601/v1

Abstract

In this study, the production of indoor humidity-buffering coatings (IHC-s) from recycling waste silica sludges by using a room-temperature sol-gel method which is a simple and energy-efficient route is reported. The properties of these IHC-s coatings are identified by scanning electron microscope, X-ray diffraction, X-ray fluorescence spectrometer, laser particle size analyzer, N_2 adsorption-desorption isotherms and toxicity characteristic leaching procedure (TCLP). The moisture adsorption-desorption tests show that the IHC-s coatings have moisture buffering values of ca. 270-316 g m^{-2} and moisture contents of 24-27% in the range of 50-90% relative humidity (RH). Furthermore, the humidity buffering capacities, moisture adsorption-desorption rate and stability are significantly superior to commercially available coatings in the range of 50-75% RH. The enhancement may be due to the formation of porous structure in the coatings *via* the dispersed waste silica sludges and gypsum which transformed from bassanite by self-assembly process. Most importantly, the prepared IHC-s coatings show surpassing antimicrobial efficacy (> 99.99%) and no detectable leaching heavy metals based on TCLP tests, which provides an economic and environmental-friendly route for recovering and valorizing industrial wastes.

Introduction

The energy consumption by buildings was estimated to be ca. 40% of global energy and over 50% of them in the buildings comes from heating and air-conditioning machines [1]. In order to cut down the CO_2 emissions from the extensive energy consumption in the buildings, the development of passive materials for the buildings that can adjust the indoor humidity naturally and keep the comfortable level of living environment is crucial [2–4]. In Taiwan, the average annual relative humidity (RH) is usually higher than 75%, which much higher than the suitable RH (40–70%) for people [5]. Therefore, dehumidifiers which consume a large amount of energy are commonly used to regulate indoor RH [6]. To have a better living space, it is urgent to create an energy-saving technology for the control of indoor humidity. The humidity buffering materials (HBMs) have attracted much attraction due to its zero-energy consumption [7–14]. Generally, the diatomite [15, 16] is frequently used as starting materials to fabricate HBMs because of its superior properties such as low toxicity, lightweight, abundance and high porosity [17–22]. For example, it was proposed that HBMs were prepared by high-temperature sintering diatomite with volcanic ash [23]. Escalera et al. [15] reported that the sintering of diatomite with Brazil nut shell ash to produce brick-type HBMs. In the recent years, many different materials were developed for HBMs applications. The synthesis of metal-organic frameworks (MOFs) [24, 25] which have larger surface area (S_{BET}) and pore volume (V_{total}) was reported and tested as HBMs for moderating indoor moisture variation. A smart wall-brick HBM prepared from sepiolite and $CaCl_2$ exhibits a superior adsorption-desorption content with antifouling and antifungal properties [26]. Bioinspired ant-nest-like hierarchical porous materials were proposed for narrowing indoor humidity fluctuation [27]. A renewable bamboo charcoal loaded with silver doped titanium dioxide was prepared and served as HBMs to improve indoor environment quality [28]. However, the aforementioned HBMs may suffer from the energy-intensive and complex preparation routes as well

as high cost. To fulfil the large-scale applications, the development of a simple, rapid, low-temperature and cost-effective method to prepare HBMs should be highlighted.

It was estimated that ca. 5.5 million tons of industrial inorganic sludges were generated annually in Taiwan. Landfills are the common methods for practical treatments of these wastes. Although the sludges may be recycled as soil additives, adsorbents and construction materials [29–31], the recovery ratios and amounts are still low until now. In this way, some environmental problems, for instance, the overload of landfill and improper disposal may happen. Form the viewpoint of circular economy, an economic feasible and environmental friendly method should be developed to recover these industrial wastes efficiently.

In this work, the indoor humidity-buffering coatings (IHC-s) were fabricated by recovering industrial sludges (*i.e.*, waste silica sludges) which were generated from precipitated silica producing plants. The physicochemical properties of waste silica sludges and prepared IHC-s were investigated by employing a series of analytic techniques and spectroscopic instruments. Humidity buffering performance of the prepared IHC-s was explored by moisture adsorption-desorption tests. Additionally, toxicity characteristic leaching tests of these IHC-s were also performed. The performance comparison between the prepared IHC-s with commercially available coatings was carried out.

Materials And Methods

IHC-s fabrication

Industrial waste silica sludges were obtained from the plants which produced precipitated silica in Taiwan. As can be seen in Fig. 1, the waste silica sludges were dried at 105^{o}C for 2 d and grounded to the powders which were sieved with a filter of 100 mesh. The IHC-s was prepared by using a facile sol-gel method. In a typical run, the weighed waste silica sludges (0–60 g), bassanite (35–90 g) and kaolin (5 g) were mixed entirely. The sodium silicates (5 g) and acrylic resins (65 g) were totally liquefied in deionized water and then sol-gelled together with aforementioned components. The humidity buffering properties were studied based on the recovery ratios of waste silica sludges, *i.e.*, the prepared IHC-s (s = weight percentages (%) of waste silica sludges). The commercial coatings made of diatomite were obtained from Econ-phoenix Company. The main chemical compositions of commercial coatings can be seen in Table S1.

IHC-s Characterizations

Morphologies of prepared samples were investigated by scanning electron microscope (SEM, AURIGA). Chemical structures of samples were identified by a variety of spectroscopies, i.e., X-ray diffraction (XRD, PANalytical X'Pert PRO), X-ray fluorescence spectrometer (XRF, PANalytical Epsilon 4), laser particle size analyser (Beckman Couter LS-230) and N_2 adsorption-desorption isotherms (Micromeritics ASAP 2020). Toxicity characteristic leaching procedure (TCLP) tests were carried out by employing the standard

method (NIEA R201.14C). The heavy metals of waste silica sludges and coatings were identified by inductively coupled plasma-optical emission spectrometer (ICP-OES, JY ULTIMA 2000).

Humidity buffering performance

To perform moisture adsorption-desorption tests, the IHC-s were covered onto the plate (100 mm x 100 mm) with the coating thickness of 2 mm. Humidity buffering properties of coatings were evaluated by moisture adsorption-desorption tests and response to humidity variation. For moisture adsorption-desorption tests, three different coatings were fabricated, dried and weighted (m_o). Before moisture adsorption, the coatings were cured at 25°C under 50% RH for 48 h. Afterwards, moisture adsorption and desorption of these coatings were carried out at 90% and 50% RH, respectively. As a result, the weights of moisture adsorption (m_{a1} and m_{a2}) and desorption (m_{d1} and m_{d2}) can be obtained. The moisture adsorption capacities of coatings (m_1, m_2, m_3 and m_4) were calculated based on the following equations (1–4). Accordingly, moisture buffering capacities (W_a, g m^{-2}) are attained by taking the averaged values by using Eq. (5).

$m_1(g) = m_{a1} - m_0$ (1)

$m_2(g) = m_{a1} - m_{d1}$ (2)

$m_3(g) = m_{a2} - m_{d1}$ (3)

$m_4(g) = m_{a2} - m_{d2}$ (4)

$$W_a = \frac{m_1+m_2+m_3+m_4}{4\times A} \quad (5)$$

where A (m^2) is the surface area of prepared coatings.

Furthermore, moisture adsorption content (u) can be obtained according to Eq. (6).

$$u(\%) = \frac{m_1-m_0}{m_0} \quad (6)$$

where m_0 is the sample weight after drying and m_1 is the sample weight after moisture adsorption.

For response to humidity variation, the adsorption-desorption of moisture was conducted in the humidity range of 50–75% RH, *i.e.*, moisture adsorption at 75% RH for 24 h and then desorption at 50% RH for 24 h. Hygroscopic sorption properties of coatings was investigated by measuring moisture contents of coatings in different RH (40, 50, 75, 85 and 90%). Durability of coatings was also performed *via* four cyclic moisture adsorption-desorption tests for at least 96 h in the range of 50–75% RH.

Results And Discussion

Textural properties of waste silica sludges

Industrial waste silica sludges, which their main chemical compositions are shown in Table S1, are the key raw materials for the IHC-s. As observed, the dominant chemical element of waste silica sludges is silicon (ca. 98.8%) which is originated from the manufacture of precipitated silica. Additionally, a small amount of sulfur elements (ca. 0.98%) observed in the waste silica sludges is attributed to the usage of sulfuric acid during the process. Some heavy metals such as calcium, alumina, iron, magnesium, copper and arsenic are found in the waste silica sludges. As shown in Fig. 2. the waste silica sludges have a broad XRD diffraction peak at $2\theta = 22^{o}$, indicating the existence of amorphous silica [32]. As observed in Fig. 3a, the particle size of waste silica sludges is mostly located between 10 and 50 μm. The averaged particle size of waste silica sludges is calculated to be ca. 26.8 μm. The SEM image (Fig. 3b) of waste silica sludges show the formation of aggregated silica particles with amorphous structure. The porous structure of waste silica sludges (i.e., specific S_{BET} and V_{total}) were determined by N_2 adsorption at 77 K and the results are summarized in Table S2. The result shows that waste silica sludges have a S_{BET} of 58.7 $m^2\ g^{-1}$ and V_{total} of 0.64 $cm^3\ g^{-1}$. In addition, waste silica sludges exhibit a type-IV isotherm (Fig. 3c) with pore size distribution of 10–100 nm (Fig. 3d). The presence of meso-macropore in the waste silica sludges is responsible for the moisture adsorption and desorption performance as discussed in the following section.

Physicochemical properties of IHC-s

As reported earlier [33], transformation of $CaSO_4{\cdot}0.5H_2O$ (bassanite) into $CaSO_4{\cdot}2H_2O$ (gypsum) *via* self-assembly process (as indicated in the Eq. (7)) and the formed gypsum can serve as the skeleton structure which provides mechanical properties such as hardness, compressive strength and porosity for the coating.

$$CaSO_4{\cdot}0.5H_2O + nH_2O \rightarrow CaSO_4{\cdot}2H_2O + (n\text{-}1.5)\ H_2O \quad (7)$$

As shown in Fig. 4a and b, the bassanite with the brick-like morphology is hydrated into gypsum with rod-like particles during casting process. The gypsum with rod-like particles is also observed for IHC-0 (without waste silica sludges), as can be seen in Fig. 4c. This indicates that the crystallization of gypsum can occur even in the existence of the acrylic resin, which also can be confirmed by XRD pattern (see Fig. 2). The characteristic peaks of gypsum are located at 11.6°, 20.7°, 23.3°, 26.6°, 29°, 31°, 33.4°, 35.9° and 40.6°, suggesting the formation of gypsum in the IHC-s. The waste silica sludges is an amorphous SiO_2 with micro-sized particles which can suspend completely in the water. The dissolution of SiO_2 (0.01–0.012% by weight in water at $25^{o}C$) produces monomeric form, *i.e.*, $Si(OH)_4$ and the solid phase [34]. The dispersed waste silica sludges in the solvent can be adhered by the resin and then consolidate between the cross-linking structure of rod-like particles of gypsum, as shown in Fig. 4d. The mesoporous and microporous structure can be developed by the dispersed waste silica sludges and gypsum. Therefore, the higher ratios of waste silica sludges can supply more mesopore for the IHC-s coatings. However, the excessive waste silica sludges (> 60 wt%) can make coating surface crack, as displayed in Fig. 5. In addition, the surface cracking also may be due to the insufficiency of gypsum, which make the skeleton

weak and thus excessive agglomeration of waste silica sludges by resins. In this study, different ratios (0–58 wt%) of waste silica sludges were used and fabricated as IHC-s.

The porous structure of IHC-s and commercial coatings is investigated by N_2 adsorption-desorption isotherms. All the samples exhibit Type-IV isotherms due to the presence of mesoporous structure, as can be seen in Fig. 6a. Also, the Type-H3 hysteresis loops can be observed for IHC-s with different amounts of waste silica sludges because slit-shaped pores are formed in the presence of gypsum and waste silica sludges particles. Accordingly, specific S_{BET} and the V_{total} of IHC-s with different ratios of waste silica sludges and commercial coatings are summarized in Table 1. As a result, the S_{BET} and V_{total} of coatings are increased as the ratios of waste silica sludges are increased. The S_{BET} values f IHC-s (s = 38, 48 and 58 wt%) are measured to be 10.0, 13.1 and 13.5 $m^2 g^{-1}$, respectively, which are larger than original IHC-0 (3.9 $m^2 g^{-1}$) and commercial coatings (2.0 $m^2 g^{-1}$). The V_{total} values are also increased as amounts of waste silica sludges are increased (from 0.049 to 0.206 $cm^3 g^{-1}$). The above result suggests that the addition of waste silica sludges can increase the V_{total} and S_{BET}. It should be noted that the total volume of commercial coatings is greater than those of IHC-s. However, pore volumes of commercial coatings are mostly attributed to the contribution of macropore (> 50 nm). Moreover, the mesopores (*i.e.*, 2–50 nm) in the IHC-s are the most effective pores for moisture adsorption. Therefore, the presence of waste silica sludges can increase the volumes of mesopores, as evidenced in the pore size distributions of IHC-s (see Fig. 6b).

Table 1
Porous properties of IHC-s samples

Samples	IHC-0	IHC-38	IHC-48	IHC-58	Commercial coatings
S_{BET} ($m^2 g^{-1}$)	3.9	10.0	13.1	13.5	2.0
V_{total} ($cm^3 g^{-1}$)	0.049	0.147	0.193	0.206	0.505

Surface contact angles of IHC-s samples are shown in Fig. 7. The adsorption time relates to the porous properties of materials, *i.e.*, the faster rate of water drop adsorption the higher porosity of samples. The pristine IHC-0 shows lower adsorption rate that the water drop cannot be adsorbed completely over 130 s. Upon adding waste silica sludges, the initial contact angles become smaller and the adsorption rates for water drop are increased. Therefore, the more ratios of waste silica sludges result in the increased pore volumes that promote the ability for liquid water adsorption.

Moisture adsorption-desorption capacity tests

The moisture buffering performance (in the range of 50–90% RH) of the IHC-s is shown in Table 2. The moisture buffering capacities and content values of IHC-0 are 216.9 g m^{-2} and 16.3%, respectively. The moisture buffering capacities of IHC-s gradually increase as the amounts of waste silica sludges increase, *i.e.*, the performance of samples with waste silica sludges is better than that of IHC-0. As a result, the moisture buffering capacities of IHC-38, IHC-48 and IHC-58 can reach 270.3, 303.7 and 316.1 g

m^{-2}, respectively. Also, moisture contents of IHC-38, IHC-48 and IHC-58 are 23.6, 25.6 and 26.7%, respectively. The moisture buffering capacities and contents of IHC-s are remarkably superior to those of commercially available coatings (58.7 g m^{-2} and 11.4%), which are possibly due to the unique porous properties. Moisture buffering ability has the positive correlation with S_{BET} and V_{total} of coatings.

Table 2
Moisture buffering capacities and contents of IHC-s and commercial coating

Sample	IHC-0	IHC-38	IHC-48	IHC-58	Commercial coatings
W_a (g m^{-2})	216.9	270.3	303.7	316.1	58.7
u (%)	16.3	23.6	25.6	26.7	11.4

Humidity buffering performance (in the range of 50–75% RH) of IHC-s and their corresponding results are shown in Fig. 8a. Except to IHC-0 coating, IHC-s (s = 38, 48 and 58%) have the higher moisture buffering capacities in the range of 50–75% RH, indicating the waste silica sludges possess the positive effect on moisture adsorption. In addition, the benchmarks of adsorbed capacities for HBMs issued by Japanese Industrial Standards (JIS, see Table S3) are 29 g m^{-2} (Level 1) and 50 g m^{-2} (Level 2) for the adsorption time of 12 h. The IHC-38, IHC-48 and IHC-58 samples possess moisture buffering capacities of 48.6, 48.4 and 46.1 g m^{-2}, respectively for the adsorption time of 12 h, which reach the requirement of Level 1 and close to Level 2. Also, adsorption-desorption gradients of various coatings are shown in Fig. 8b. The IHC-48 coatings have the highest adsorption rate (20.1 g m^{-2} h^{-1}) and the optimal desorption rate can be observed for IHC-38 (-17.3 g m^{-2} h^{-1}). The results show that the adsorption and desorption rates of IHC-s (s = 38–58%) are higher than that of IHC-0 and commercial coatings. Hygroscopic curves of the IHC-s coatings are shown in Fig. 8c. The IHC-48 coatings start to adsorb moisture at the RH of 40%. It can be seen that no significant difference between IHC-48 and commercial coatings can be observed in the humidity range of < 50%. While relative humidity are higher than 75%, the adsorbed capacities are increased sharply upon the addition of waste silica sludges. Note that curves of adsorption and desorption are not overlapped due to the hysteresis effect. Durability of adsorption-desorption process for IHC-48 was performed by cyclic tests, as presented in Fig. 8d. The moisture buffering capacities of IHC-48 coatings keep stable for four cyclic runs (*i.e.*, the entire run time = 96 h). In other words, the moisture can be adsorbed by IHC-48 spontaneously and then desorbed from pores entirely.

As shown in Table S4, leaching contents of heavy metals (Cu, Cr, Cd, Ni, Ba, Co and Pb) for IHC-48 were investigated by the TCLP tests. No detectable heavy metals are observed in leaching solutions of IHC-48 coatings. Moreover, the antibacterial property of IHC-48 is evaluated *via* the standard method from JIS (JIS Z 2801). As observed in Table S5, the bacteria concentration of 99 CFU mL^{-1} observed for IHC-48 after the contact time of 24 h is significantly lower 6.0 × 10^6 CFU mL^{-1} for blank. The R factor of antimicrobial activity is ca. 4.8 which is greater than the threshold value (*i.e.*, 2) of Japanese Industrial Standards (JIS Z 2801). It is worthy to note that the IHC-48 recycled from industrial wastes possesses an excellent moisture buffering ability which can reach the benchmark of Japanese Industrial Standards and is also superior to the commercial coatings. More importantly, the simple and energy-saving sol-gel

method to prepare IHC-48 coatings with an excellent antimicrobial efficacy (> 99.99%) and environmental friendliness (non-detectable heavy metal leaching) recycled from inorganic wastes under room temperature may be a promising candidate for practical applications in the indoor coatings.

Conclusions

The humidity buffering coatings, which are the new application of controlling indoor humidity, is prepared by using a room-temperature sol-gel method from recovering industrial wastes in this study. These IHC-s coatings fabricated by using different ratios of resins, basanite, kaolin, sodium silicates and waste silica sludges exhibit moisture buffering values of ca. 270–316 g m^{-2} and moisture contents of 24–27% in the range of 50–90% RH. Moreover, the prepared IHC-s coatings can meet the JIS Level 2 criteria in the range of 50–75% RH. Compared to commercially available coatings, our IHC-s coatings have excellent humidity buffering properties (moisture capacity, adsorption-desorption rate and durability) and in the high and medium humidity range. Most importantly, the IHC-s coatings with superior antibacterial property are produced by using an energy-saving route and healthy to human without the leaching of heavy metals. The study also demonstrates the valorization of industrial sludges to produce indoor coatings with high humidity buffering ability and low cost that are potentially applied in our circular economy society.

Declarations

Availability of data and materials

All data supporting the conclusions of this article are included in this manuscript.

Competing interests

The authors declare they have no competing interests.

Funding

This work was supported by Ministry of Science and Technology of Taiwan (MOST 107-2221-E-006-009-MY3).

Authors' contributions

C.-H.K.: Methodology, Investigation, Data curation, Writing - original draft; W.D.: Data curation, Writing - review & editing; S.-H.L.: Conceptualization, Writing - review & editing, Supervision, Project administration

Acknowledgments

We are gratefully appreciated the support of this study by the Ministry of Science and Technology of Taiwan.

References

1. Hou PM, Zu K, Qin MH, Cui SQ. A novel metal-organic frameworks based humidity pump for indoor moisture control. Build. Environ. 2021;187:107396.
2. Kreiger BK, Srubar WV. Moisture buffering in buildings: A review of experimental and numerical methods. Energy Build. 2019;202:109394.
3. Wan H, Sun ZW, Huang GS, Xu XH, Yu JH. Calculation of the maximum moisture buffering thickness of building wall layer of hygroscopic material. Build Environ. 2019;160:106173.
4. Park JH, Kim YU, Jeon J, Yun BY, Kang Y, Kim S. Analysis of biochar-mortar composite as a humidity control material to improve the building energy and hygrothermal performance. Sci Total Environ. 2021;775:145552.
5. Lin YW, Cheng, TW, Lo KW, Chen CY, Lin KL. Synthesis and characterization of a mesoporous Al-MCM-41 molecular sieve material and its moisture regulation performance in water molecule adsorption/desorption. Microporous Mesoporous Mater. 2021;310:110643.
6. Gurubalan A, Simonson JC. A comprehensive review of dehumidifiers and regenerators for liquid desiccant air conditioning system. Energy Convers. Manage. 2021;240: 114234.
7. Wang XZ, Gao WY, Yan SA, Niu MH, Liu GH, Hao HS. Incorporation of sand-based breathing bricks with foamed concrete and humidity control materials. Construct Build Mater. 2018;175:187–195.
8. Lee H, Ozaki A, Lee M, Yamamoto T. Humidity control effect of vapor-permeable walls employing hygroscopic insulation material. Indoor Air 2020;30:346–360.
9. Maria I, Petrisor S, Corneliu C, Gabriela S, Igor C, Valeria H. Porous polymer/inorganic composite matrices as efficient desiccants for air dehumidification. Appl Surf Sci. 2019;487:1189–1197.
10. Novais RM, Carvalheiras J, Senff L, Lacasta AM, Cantalapiedra IR, Giro-Paloma J, et al. Multifunctional cork - alkali-activated fly ash composites: A sustainable material to enhance buildings' energy and acoustic performance. Build Environ. 2020;210:109739.
11. Shi CN, Zhang HB, Xuan Y. Experimental investigation of thermal properties and moisture buffering performance of composite interior finishing materials under different airflow conditions. Build Environ. 2019;160:106175.
12. Tsobnang PK, Hasturk E, Frohlich D, Wenger E, Durand P, Ngolui JL, et al. Water vapor single-gas selectivity via flexibility of three potential materials for autonomous indoor humidity control. Cryst Growth Des. 2019;19:2869–2880.
13. Wang YA, Chen Y, Wang JM, Xv XC, Yang X, Zhou J, et al. Novel porous ultrathin NiO nanosheets for highly efficient water vapor adsorption-desorption. Sep Purif Technol. 2019;226:299–303.
14. Lu HC, Kuok CH, Liu SH. High-performance humidity control coatings prepared from inorganic wastes. Construct Build Mater. 2020;263:120169.
15. Escalera E, Garcia G, Terán R, Tegman R, Antti ML, Odén M. The production of porous brick material from diatomaceous earth and Brazil nut shell ash. Construct Build Mater. 2015;98:257–264.

16. Hu ZB, Zheng SL, Sun ZM, Chen Y, Yan Y. Influence of pore structure on humidity control performance of diatomite. Sci Technol Built Environ. 2017;23:1305–1313.
17. Fraine Y, Seladji C, Ait-Mokhtar A. Effect of microencapsulation phase change material and diatomite composite filling on hygrothermal performance of sintered hollow bricks. Build Environ. 2019;154:145–154.
18. Hu ZB, Zheng SL, Jia MZ, Dong XB, Sun ZM. Preparation and characterization of novel diatomite/ground calcium carbonate composite humidity control material. Adv Powder Technol. 2017;28:1372–1381.
19. Hu ZB, Zheng SL, Tan Y, Jia MZ. Preparation and characterization of diatomite/silica composite humidity control material by partial alkali dissolution. Mater Lett. 2017;196:234–237.
20. Konuklu Y, Ersoy O, Gokce O. Easy and industrially applicable impregnation process for preparation of diatomite-based phase change material nanocomposites for thermal energy storage. Appl Therm Eng. 2015;91:759–766.
21. Wu ZM, Qin MH, Zhang MJ. Phase change change humidity control material and its impact on building energy consumption. Energy Build. 2018;174:254–261.
22. Zheng JY, Shi J, Ma Q, Dai XL, Chen ZQ. Experimental study on humidity control performance of diatomite-based building materials. Appl Therm Eng. 2017;114:450–456.
23. Vu DH, Wang KS, Bac BH, Nam BX. Humidity control materials prepared from diatomite and volcanic ash. Construct Build Mater. 2013;38:1066–1072.
24. Cui SQ, Qin MH, Marandi A, Steggles V, Wang SJ, Feng XX, et al. Metal-Organic Frameworks as advanced moisture sorbents for energy-efficient high temperature cooling. Sci Rep. 2018;8:15284.
25. Feng XX, Qin MH, Cui SQ, Rode C. Metal-organic framework MIL-100(Fe) as a novel moisture buffer material for energy-efficient indoor humidity control. Build Environ. 2018;145:234–242.
26. Liu XP, Chen Z, Yang G, Zhang ZT, Gao YF. Colorful wall-bricks with superhydrophobic surfaces for enhanced smart indoor humidity control. ACS Omega 2019;4:13896–13901.
27. Liu XP, Chen Z, Yang G, Gao YF. Bioinspired ant-nest-like hierarchical porous material using $CaCl_2$ as additive for smart indoor humidity control. Ind Eng Chem Res. 2019;58:7139–7145.
28. Ren Q, Zeng ZY, Jiang ZW, Chen Q. Incorporation of bamboo charcoal for cement-based humidity adsorption material. Construct Build Mater. 2019;215:244–251.
29. Wang L, Chen L, Cho DW, Tsang DCW, Yang J, Hou D, et al. Novel synergy of Si-rich minerals and reactive MgO for stabilisation/solidification of contaminated sediment. J Hazard Mater. 2020;365:695–706.
30. Florent M, Policicchio A, Niewiadomski S, Bandosz TJ. Exploring the options for the improvement of H_2S adsorption on sludge derived adsorbents: Building the composite with porous carbons. J Clean Prod. 2020;249:119412.
31. Ngo TNLT, Chiang KY. Co-thermal degradation characteristics of rice straw and sewage sludge. Sustain Environ Res. 2021;31:23.

32. Buhani, Wijayanti TA, Suharso, Sumadi, Ansori M. Application of modified green algae Nannochloropsis sp. as adsorbent in the simultaneous adsorption of Methylene Blue and Cu(II) cations in solution. Sustain Environ Res. 2021;31:17.
33. Van Driessche AES, Benning LG, Rodriguez-Blanco JD, Ossorio M, Bots P, Garcia-Ruiz JM. The role and implications of bassanite as a stable precursor phase to gypsum precipitation. Science 2012;336:69–72.
34. Alexander GB, Heston WM, Iler RK. The solubility of amorphous silica in water. J Phys Chem. 1954;58:453–455.

Figures

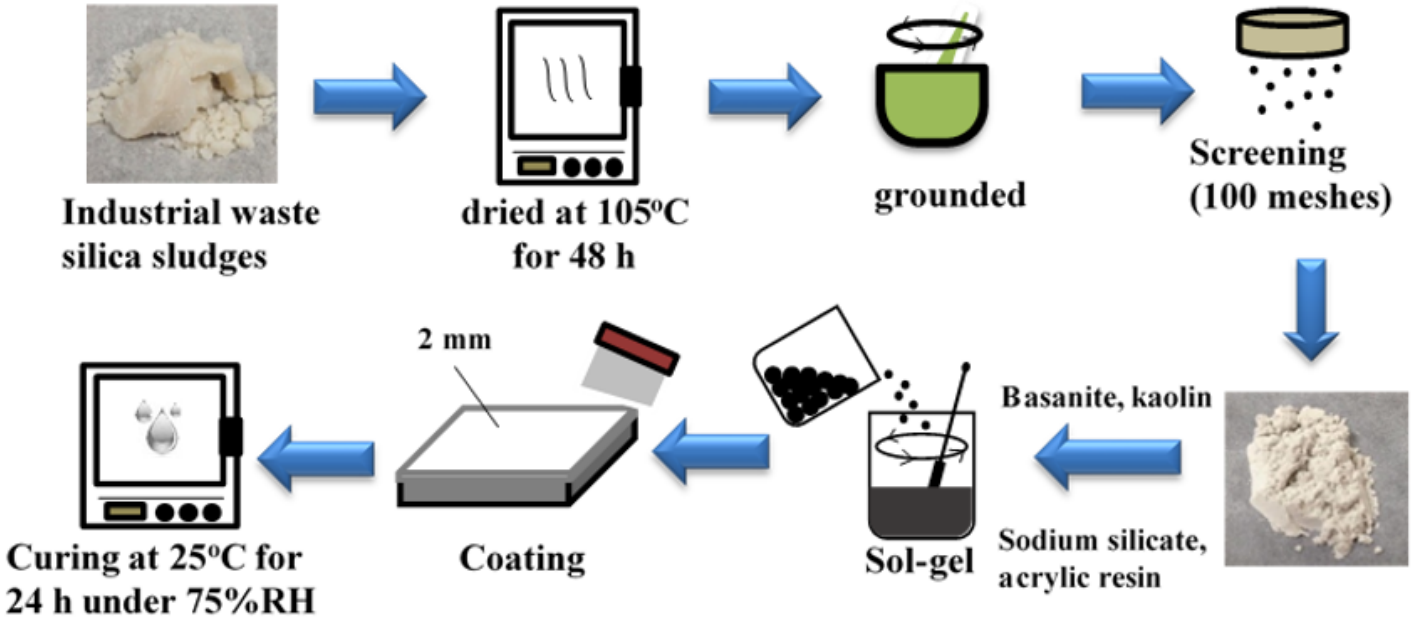

Figure 1

A schematic diagram of IHC-s preparation

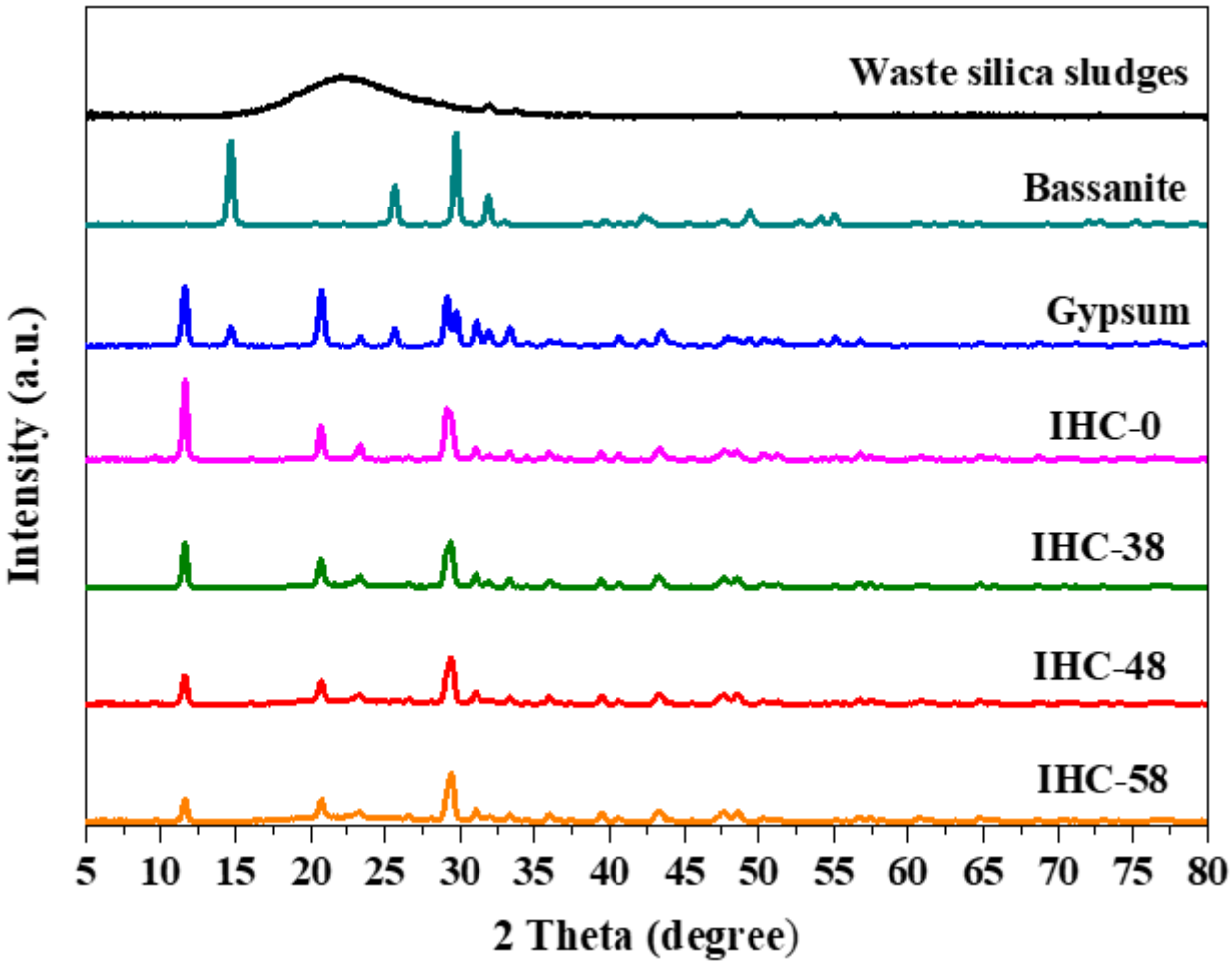

Figure 2

XRD pattern of waste silica sludges, bassanite, gypsum and IHC-s

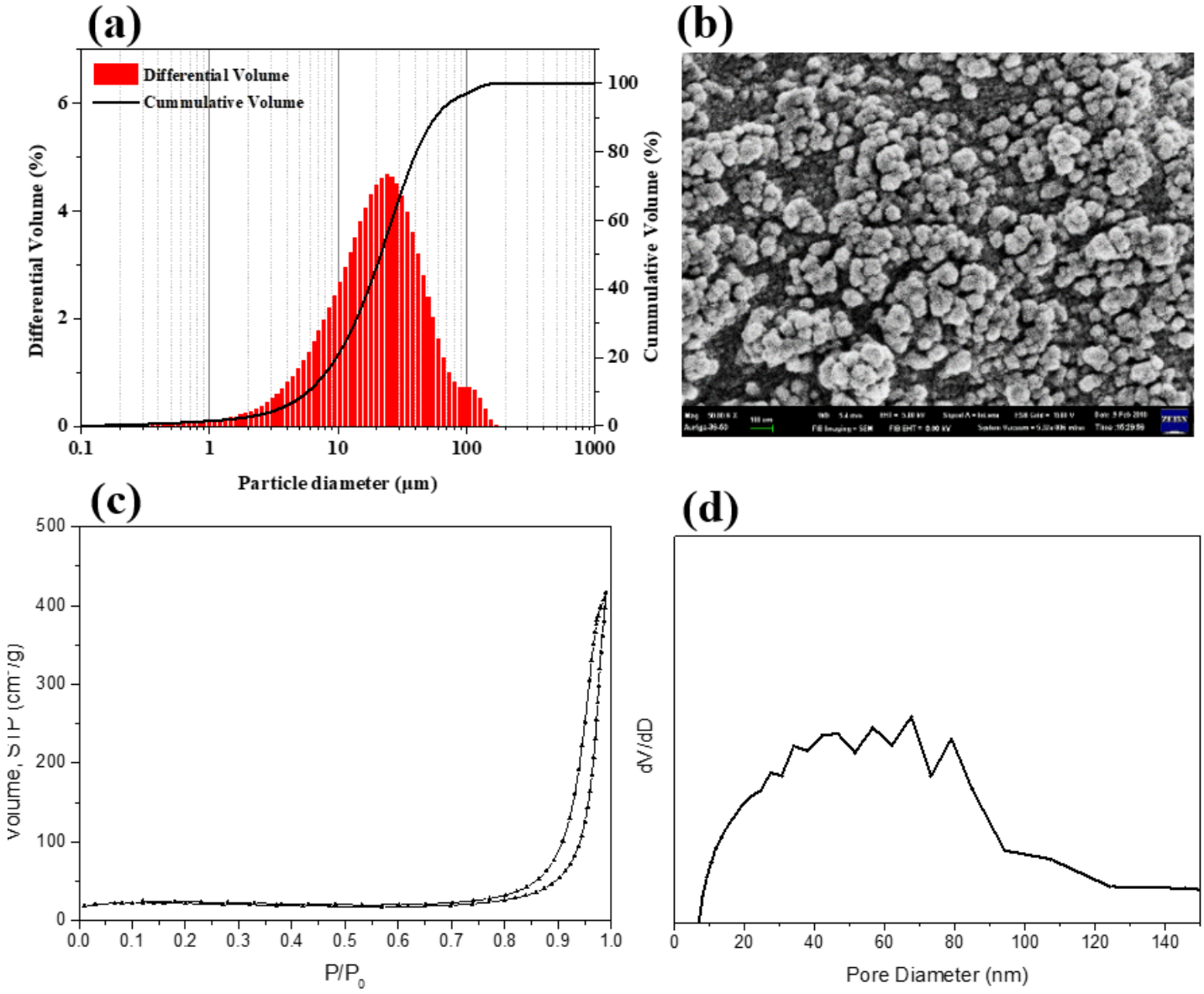

Figure 3

(a) particle size distribution, (b) SEM image, (c) N2 adsorption-desorption isotherms and (d) pore size distributions of waste silica sludges

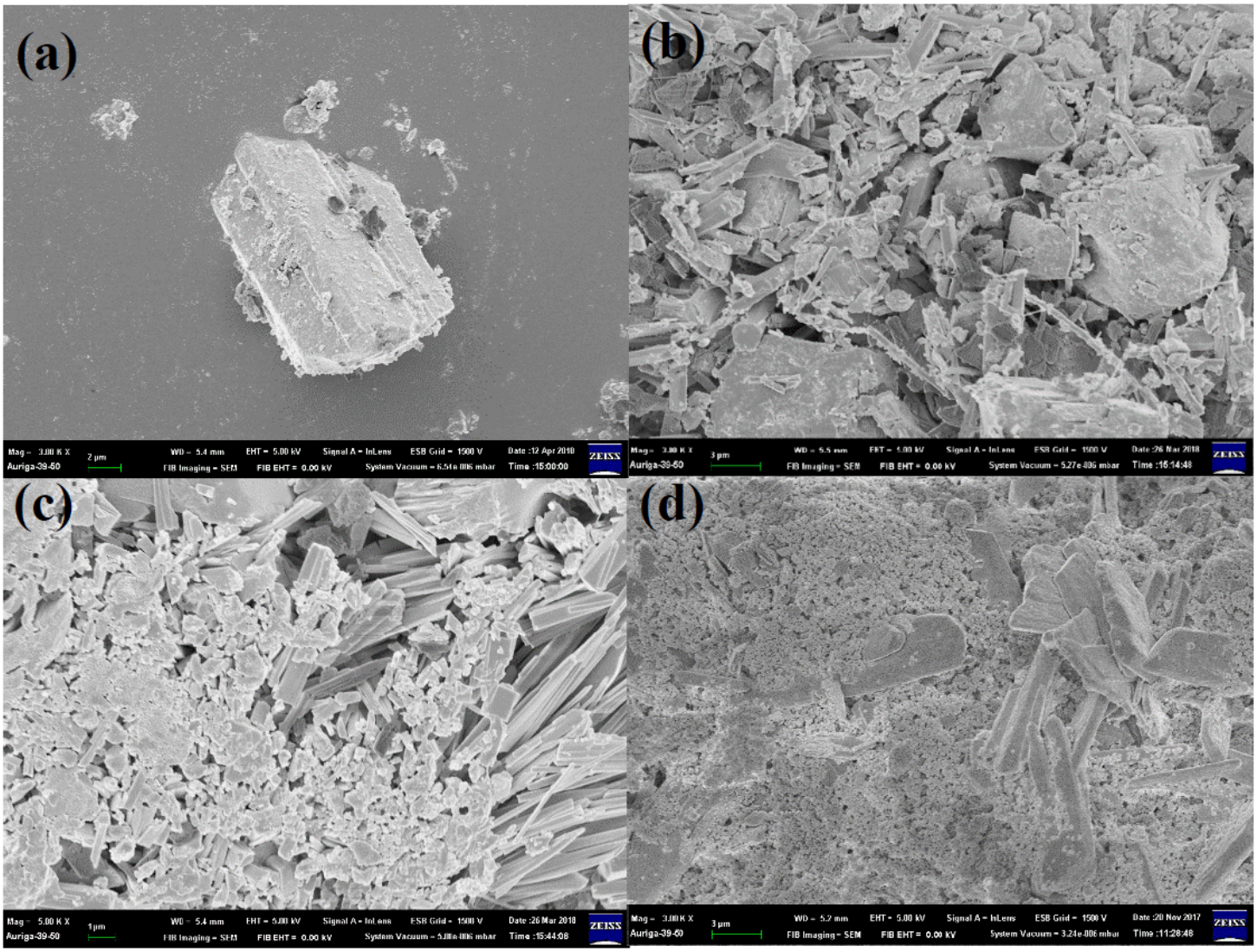

Figure 4

SEM images of (a) bassanite, (b) gypsum, and (c) IHC-0 and (d) IHC-48

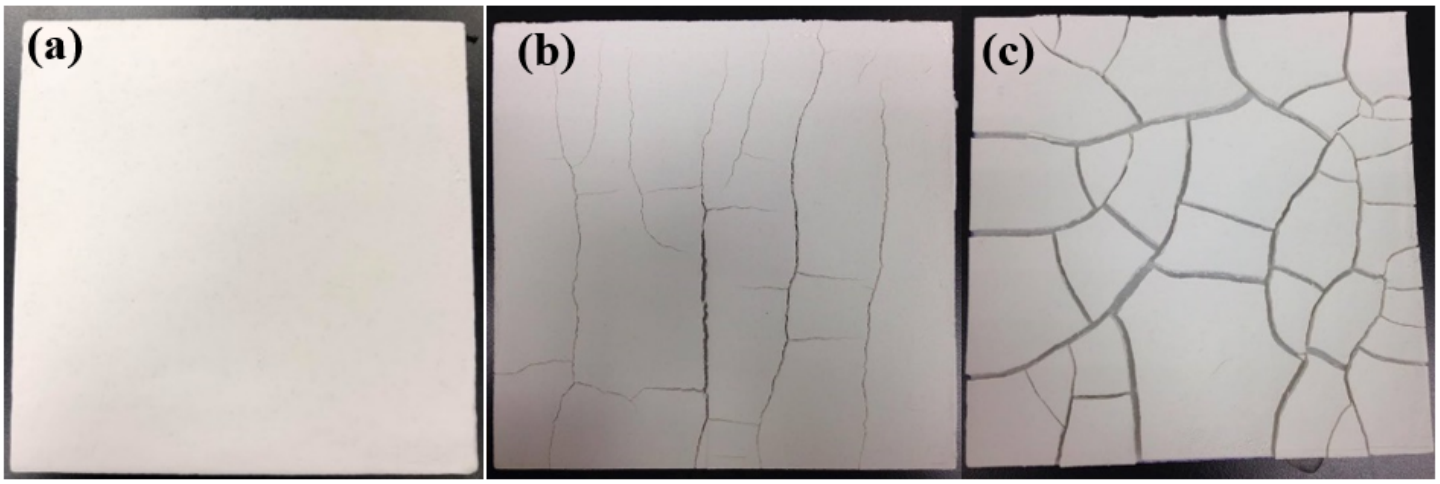

Figure 5

Photographs of (a) IHC-58, (b) IHC-78 and (b) IHC-88

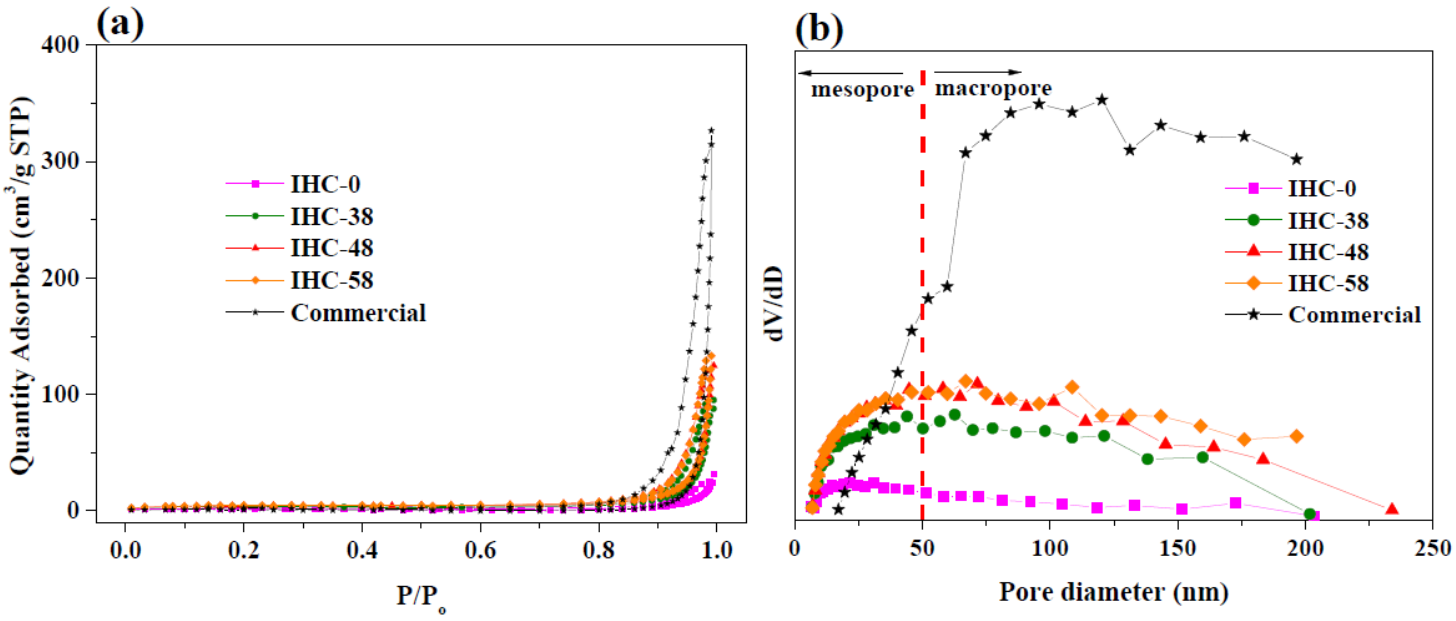

Figure 6

(a) N2 adsorption-desorption isotherms and (b) pore size distributions of IHC-s and commercial coatings

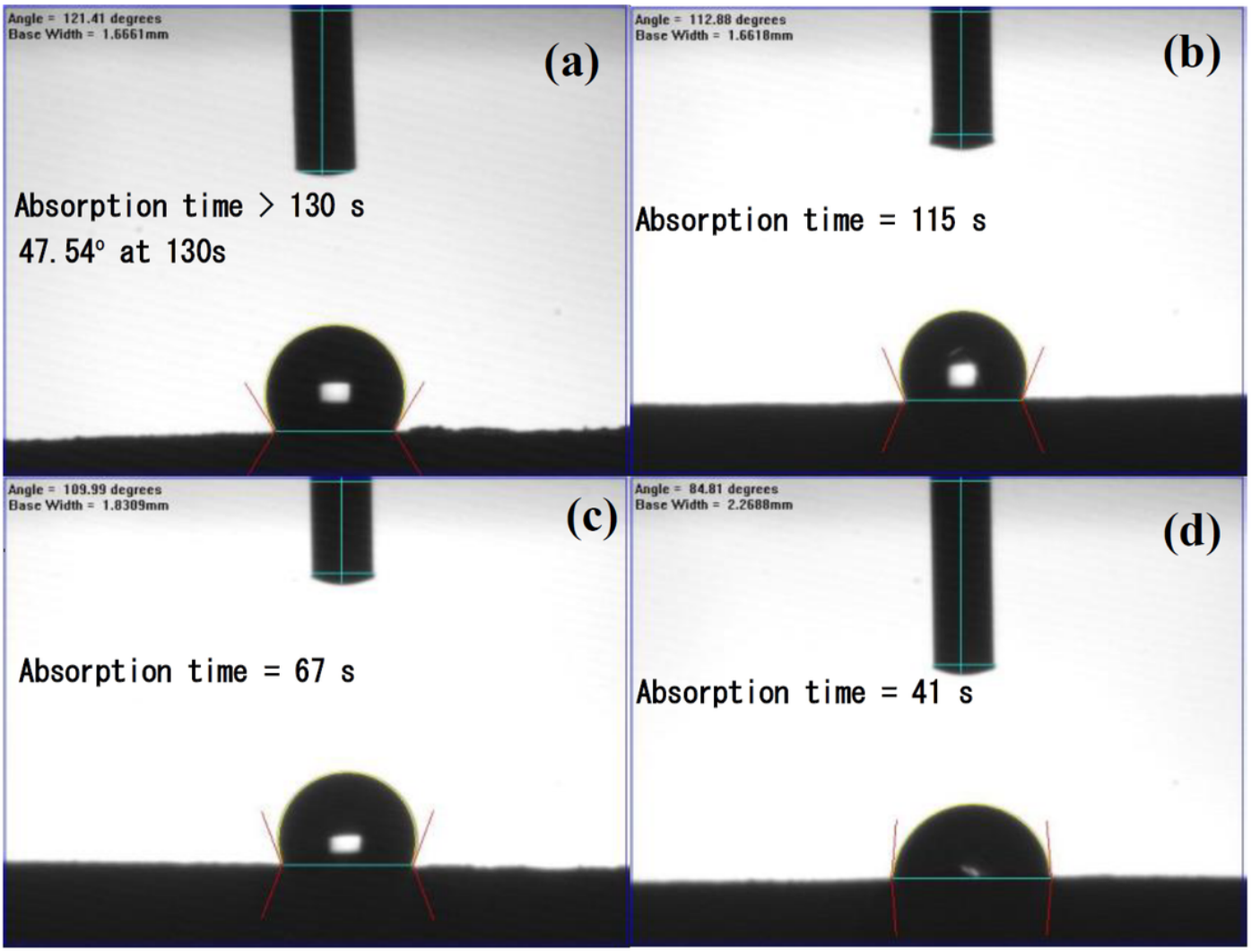

Figure 7

Surface contact angle of (a) IHC-0, (b) IHC-38, (c) IHC-48 and (d) IHC-58

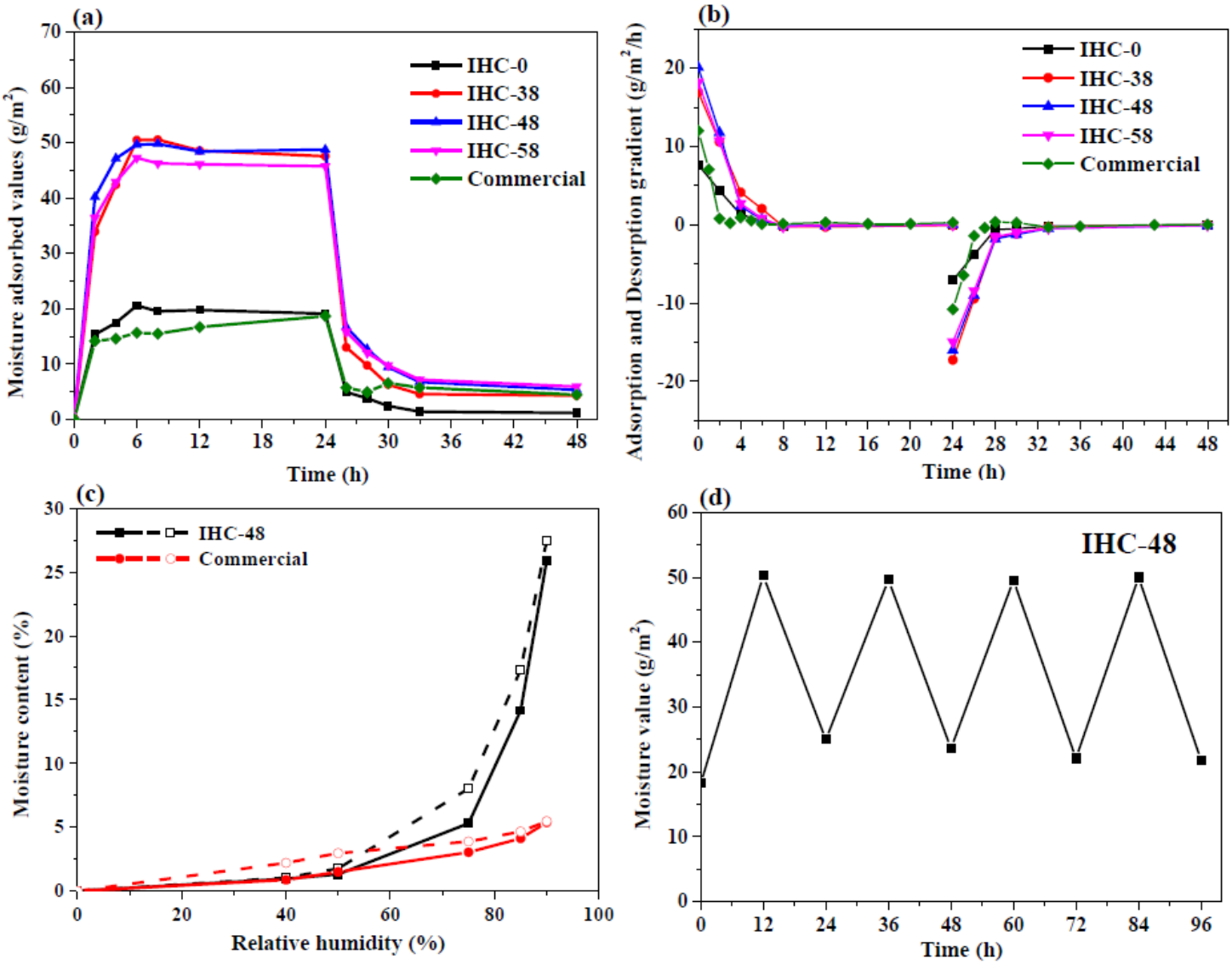

Figure 8

(a) Moisture adsorption-desorption performance, (b) gradient, (c) hygroscopic curves f IHC-s and commercial samples and (d) a cyclic test of IHC-48

Supplementary Files

This is a list of supplementary files associated with this preprint. Click to download.

- SERSupplementaryMaterial.docx